Applied Catalysis B: Environmental 333 (2023) 122783

Contents lists available at ScienceDirect

Applied Catalysis B: Environmental

journal homepage: www.elsevier.com/locate/apcatb

Fabrication of highly oxidized Pt single-atom catalysts to suppress the deep hydrogenation of unsaturated aldehydes

Yu Liang [a], Qiong Tang [a], Lei Liu [a,*], Dingsheng Wang [b], Jinxiang Dong [a]

[a] College of Chemical Engineering and Technology, Taiyuan University of Technology, Taiyuan 030024, Shanxi, China
[b] Department of Chemistry, Tsinghua University, Beijing 100084, China

ARTICLE INFO

Keywords:
Electronic configuration
Positive charge
Selective hydrogenation
Single-atom catalysts
Unsaturated aldehyde

ABSTRACT

In this work, we first reported the fabrication of single-atom Pt catalysts with high oxidation state through a mild hydrolysis method using platinum acetylacetonate as the precursor and SBA-15 coated with functional FeO_x nanoclusters as support, and evaluate their catalytic performance towards unsaturated aldehydes hydrogenation. Pt_1-FeO_x/SBA-15 featuring the high coordination number of Pt-O exhibited markedly high selectivity for hydrogenation of C═O group (> 95 %) when cinnamaldehyde conversion is 100 %, and further hydrogenation of target product could be efficiently inhibited over a prolonged period of time, and the universality of chemoselectivity was also evidenced in other unsaturated aldehydes. The experimental results and theoretical calculations revealed that the synergism of highly electron-deficient Pt single-atoms and FeO_x species is responsible for the selectivity control and the inhibition of further hydrogenation. The developed strategy offers a facile approach to the rational design of high-efficient single-atom catalysts for the selective hydrogenation with multiple intermediates.

1. Introduction

The α, β-unsaturated aldehydes (UAL) hydrogenation to α, β-unsaturated alcohols (UOL) is an critical reaction to produce fine chemicals [1,2], but achieving high yield UOL remains a grand challenge because that hydrogenation involves conjugated C═O and C═C groups in such substances, as well as the reserved C═C group in target molecules. Recently, a number of supported nanocatalysts such as noble metal of Pt and Ir, have been reported to catalyze the hydrogenation [3–5], however, these monometallic nanoparticle catalysts often exhibited poor selectivity toward UOL as the strong adsorption of C═C group on the active centers. One extensively investigated strategy is to construct intermetallic nanoparticles with noble- and transition-metal (i.e., Pt-Co, Pt-Sn, Pt-Re and Pt-Fe) to vary its electronic structure and coordination environment for improving their selectivity toward UOL [3,6–17]. However, it still failed to inhibit the further hydrogenation of the formed UOL when the conversion of UAL is getting close to the end, and these nano-sized bimetal catalysts usually exhibited low catalytic efficiency. Therefore, designing a noble metal catalyst with atomic-level dispersion and desirable electronic state is the key to acquire the excellent selectivity and high atom utilization efficiency for such reactions.

Supported single-atom catalysts (SACs) have displayed the tremendous application prospect in hydrogenation reaction with distinctive selectivity and high atom-utilization efficiency [18–23]. Among these SACs, the product selectivity was closely associated with the surface charge of the metal single-atoms [24–27]. The electronic properties are generally derived from the orbital coupling between isolated active sites and uniform support surface [28]. However, metal single atoms on support are usually obtained with a low density, the neighboring atoms around them are often absent except for the atoms in support, leading to the difficulty in adjusting its electronic properties [29,30]. Hence the precise regulation toward the electronic configuration of SACs is a challenge due to their structure simplicity. The precise regulation toward the electronic configuration of SACs is a challenge due to their structure simplicity. The strong metal-support interactions were widely designed to adjust the state of electronic on the active sites, but it set a higher request in the choice of support materials [31–38], meanwhile, these commonly applied supports (i.e., Fe_2O_3, CeO_2, WO_3 and TiO_2) usually presented a pretty low metal loading capacity on their surface due to their low surface area. Recently, novel atomically dispersed dual-atom and triple-atom catalysts (DACs and TACs) have emerged to tailor the electronic configuration of SACs or establish more active

* Corresponding author.
E-mail address: liulei@tyut.edu.cn (L. Liu).

https://doi.org/10.1016/j.apcatb.2023.122783
Received 20 February 2023; Received in revised form 16 April 2023; Accepted 18 April 2023
Available online 19 April 2023

centers for enhancing the catalytic activity or selectivity [39–41]. The reactivity of DACs was closely related to long range interactions between the two metallic centers [42], which heavily depended on the distance and matching level between them, therefore the precisely controllable synthesis of such catalysts presents an enormous challenge at current stage. More recently, Liu reported the functional CeO_x nanoclusters/nanoglues grafted on SiO_2 to construct Pt SACs, and the Pt single-atoms have high surface positive charges and high stability under reducing conditions [43]. Such catalysts combined the features of SACs and DACs. This strategy may allow researchers to design a high-efficient catalysts for those complicated hydrogenation with multiple intermediates, by selecting the functional metal oxide nanoclusters that behaved as the anchoring sites and the electronic configuration modifier for Pt species, and the active centers combining the Pt single-atom.

Among the metal precursors, organometallic complexes such as acetylacetone metal complexes, in principle, are ideal candidates for the synthesis of supported SACs [23,44–46], because the organic ligands in themselves could effectively inhibit the aggregation of metal ions on support surface during the impregnation process. The removal of ligands to expose the metal atoms is a critical step, however, the conventional methods such as high temperature calcination, tended to form metal nanoparticles under such harsh conditions [47,48]. Hence a gentle treatment approach is required for the removal of ligands, which is very crucial to obtain the isolated metal species on the support. Potential advantages based on the platinum acetylacetonate {$Pt(acac)_2$} as the precursor, herein, an atomically dispersed platinum on SBA-15 coated with FeO_x nanoclusters was successfully constructed by removing the ligands under mild hydrothermal conditions. The developed strategy is also applicable to the synthesis of other SACs (i.e., noble metal of Pd, Ir, and Rh). Pt_1-FeO_x/SBA-15 catalyst featured the highly oxidized Pt single-atoms stabilized by FeO_x nanoclusters, exhibited a remarkably high selectivity to cinnamyl alcohol (COL) (> 95 %) under the complete conversion of cinnamaldehyde (CAL), and the universality in the selectivity control was also confirmed in another UAL hydrogenation.

2. Experimental section

2.1. Synthesis of FeO_x/SBA-15

The FeO_x/SBA-15 was prepared by impregnation method with Fe $(NO_3)_3$ as precursor. The suspension with SBA-15 was stirred at room temperature, then evaporated to remove the excess solvent. The iron nitrate on the external surface of SBA-15 was thoroughly rinsed after impregnation, followed by drying at 110 °C, and calcined at 400 °C for 5 h.

2.2. Synthesis of Pt_1-FeO_x/SBA-15

Pt_1-FeO_x/SBA-15 catalysts were prepared with $Pt(acac)_2$ complex as precursor by impregnation method in ethanol solvent. The obtained FeO_x/SBA-15 was added to the $Pt(acac)_2$ solution with stirring at 50 °C for 3 h, samples were collected after ethanol was completely evaporated, which was denoted as $Pt(acac)_2$-FeO_x/SBA-15. A typical hydrolysis process involves that the required amount of $Pt(acac)_2$-FeO_x/SBA-15 water was heated at 100 °C for 12 h in a Teflon-lined reactor. The resulting product (Pt_1-FeO_x/SBA-15) was filtered and washed with water, and then drying overnight at 100 °C. For comparison, Pt/SBA-15 catalysts were prepared as described above but with SBA-15 as support, Pt-FeO_x/SBA-15-Air catalyst was also obtained by thermal treatment toward $Pt(acac)_2$-FeO_x/SBA-15 at 300 °C.

2.3. Characterizations

The HRTEM and HAADF-STEM images were recorded on JEOL JEM-2100F and FEI Talos F200x, respectively. The DRIFT experiments of CO and 3-methyl-2-butenal adsorbed on catalysts were performed on a Bruker INVENIO R spectrometer. XPS profiles were recorded on a Thermo Fisher Scientific ESCALAB 250Xi spectrometer. The XAFS data was collected at Beijing Synchrotron Radiation Facility.

2.4. Catalytic selective hydrogenation

The hydrogenation of UALs of various catalysts was evaluated in the hydrogenation. In a typical run, the calculated amount of CAL (25 mmol), catalyst (20 mg), i-PrOH (5 mL) and H_2 (3.0 MPa) were added to Teflon-lined autoclave, and then hydrogenation of UALs at room temperature. The quantitative analysis of products was conducted on gas chromatography (Shimadzu 2010 pro, FID detector and DB-5-HT column).

3. Results and discussion

3.1. Synthesis of Pt SAC by removing ligand under mild condition

The synthetic process for Pt_1-FeO_x/SBA-15 catalyst is presented in Fig. 1. First, FeO_x species were pre-formed on the channels of SBA-15 through impregnation followed by calcination. The mesoporous SBA-15 with high thermal stability and large specific surface area has an important role in controlling the dispersion of FeO_x species. Second, Pt $(acac)_2$ complex as the Pt precursor was introduced into FeO_x/SBA-15, then treated with hydrothermal approach to remove the ligand at 100 °C. The primary physicochemical parameters of SBA-15 before and after loading metal species were given in Table S1, the content of Pt and Fe determined by ICP-AES was 0.98 and 3.1 *wt*%, respectively. After incorporation of Fe and Pt species, X-ray diffraction and N_2 adsorption proved that the mesopore structure of SBA-15 was well maintained (Figs. S1 and S2), and the Fe and Pt species characteristic diffraction peaks in Pt_1-FeO_x/SBA-15 were not observed, suggesting that high dispersion of Pt and FeO_x species on the SBA-15 [49].

The removal of ligands coordinated to platinum is an indispensable step to expose Pt atoms on the support [47,48], herein, the low temperature hydrolysis of $Pt(acac)_2$ was proved to be effective and feasible in removing these ligands. By comparing thermogravimetry-mass spectrometry (TG-MS) profiles of $Pt(acac)_2$-FeO_x/SBA-15 before and after hydrolysis (Fig. S3), the absence of the thermal decomposition products (mainly CO_2) derived from $Pt(acac)_2$ in Pt_1-FeO_x/SBA-15 demonstrated that the organic species in $Pt(acac)_2$ have been successfully removed through such treatment. The Ultraviolet-visible spectroscopy indicated the characteristic peak of $Pt(acac)_2$ has been disappeared after hydrothermal treatment (Fig. S4), also verifying the success in the hydrolysis of $Pt(acac)_2$. The hydrolysis products from Pt $(acac)_2$ were also confirmed by high performance liquid chromatography (Fig. S5), which mainly consisted of acetic acid, acetone, and a trace of weakly polar species [50]. Based on these facts, it is proposed that the hydrolyzation process of $Pt(acac)_2$ may proceeded in a complicated manner (Fig. 1), the ligands attached to the metal ion were gradually dissociated to expose the platinum which was anchored the surface of FeO_x, and the ligand of acetylacetone was further hydrolyzed to acetic acid and acetone [51].

3.2. Structural characterization of Pt_1-FeO_x/SBA-15

HRTEM images proved that the uniform pore channels of SBA-15 were well maintained after loading Fe-species, and FeO_x nanoparticles (particle size > 5 nm) were not formed on SBA-15 material (Fig. 2a, b). The iron nitrate on the outside surface of SBA-15 was thoroughly rinsed after impregnation, hence FeO_x species were mainly located on the SBA-15 channels in nanoclusters after calcination. X-ray absorption spectra were performed to verify the Fe species structure. The EXAFS spectra (Fig. 3a) and the corresponding fitting results (Table S2) of the Fe K edge demonstrated the average coordination number (CN) is 2.0 for Fe-Fe shell (R of 3.01 Å), and 4.2 for Fe-O shell (R of 1.99 Å) in Pt_1-FeO_x/

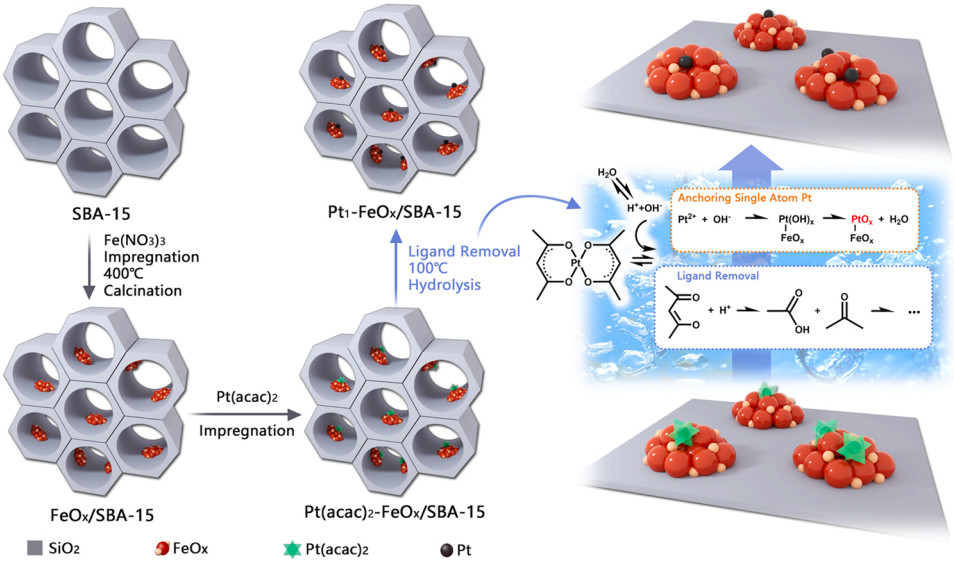

Fig. 1. Illustration of synthetic procedure of Pt_1-FeO_x/SBA-15 catalyst under mild conditions.

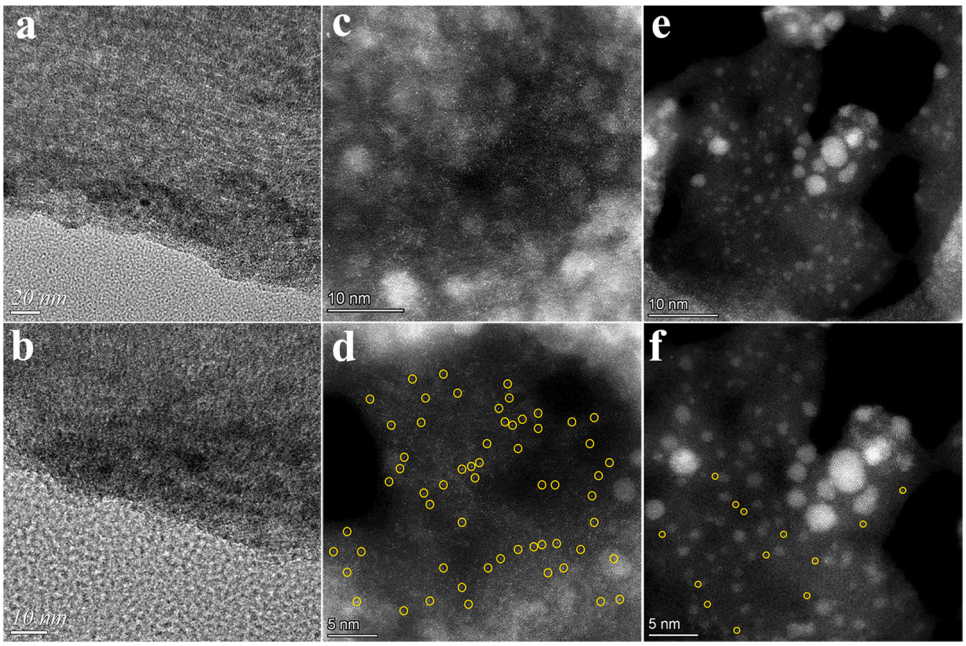

Fig. 2. (a, b) HRTEM images of FeO_x/SBA-15. HAADF-STEM images of catalysts: (c, d) Pt_1-FeO_x/SBA-15; (e, f) Pt/SBA-15.

SBA-15, which is lower than Fe-Fe in Fe foil, indicating that the catalyst possessed the unsaturated coordination of Fe species [52]. As shown in Fig. S6, the XANES profile demonstrated that the white line intensity of Pt_1-FeO_x/SBA-15 is comparable to Fe_2O_3, suggesting that the valence state of Fe is + 3. The wavelet transforms analysis (Fig. 3b) showed that the Fe—Fe and Fe—O bonds in Pt_1-FeO_x/SBA-15 are consistent with α-Fe_2O_3, but the coordination strength is weaker than that of α-Fe_2O_3, meaning that Fe species coated on SBA-15 existed in the form of α-Fe_2O_3 clusters with low-coordination, which often acted as anchor sites for the single atom platinum [53].

The HAADF-STEM was further employed to identify the atomic scale Pt species. HAADF-STEM images obviously showed that the isolated Pt atoms on FeO_x/SBA-15 uniformly (marked by yellow circles), and the single atom Pt was most likely to be deposited in the vicinity of FeO_x (Fig. 2c, d). A control experiment (Fig. 2e, f) was carried out on Pt/SBA-15 without FeO_x, in which the loaded Pt species in the form of single-atom and nanoparticles with a distribution range of 1–5 nm, showing that FeO_x nanoclusters coated on SBA-15 markedly restrained the aggregation of the Pt species derived from the hydrolysis of $Pt(acac)_2$. To verify the importance of the ligand removal through mild treatment in the construction of Pt SACs, the analogous catalyst of Pt-FeO_x/SBA-15-Air was also prepared by thermal treatment toward the $Pt(acac)_2$-FeO_x/SBA-15. As displayed in HRTEM image (Fig. S7), the Pt species tended to form the large nanoparticles on FeO_x/SBA-15, demonstrating that the mild removal of the ligand by hydrolysis is crucial to suppress the aggregation of Pt species.

To reveal the coordination environment of Pt species, EXAFS test and wavelet transform analysis were conducted on various catalysts and references. The Pt L_3 edge EXAFS profiles (Fig. 3c) show that there is a prominent Pt-O contribution peak (~ 1.7 Å) and a Pt-Pt contribution peak (2.5 Å) in R space [54]. Pt_1-FeO_x/SBA-15 mainly exhibits a large peak around 2.0 Å in EXAFS spectra, indicating that most of the Pt atoms

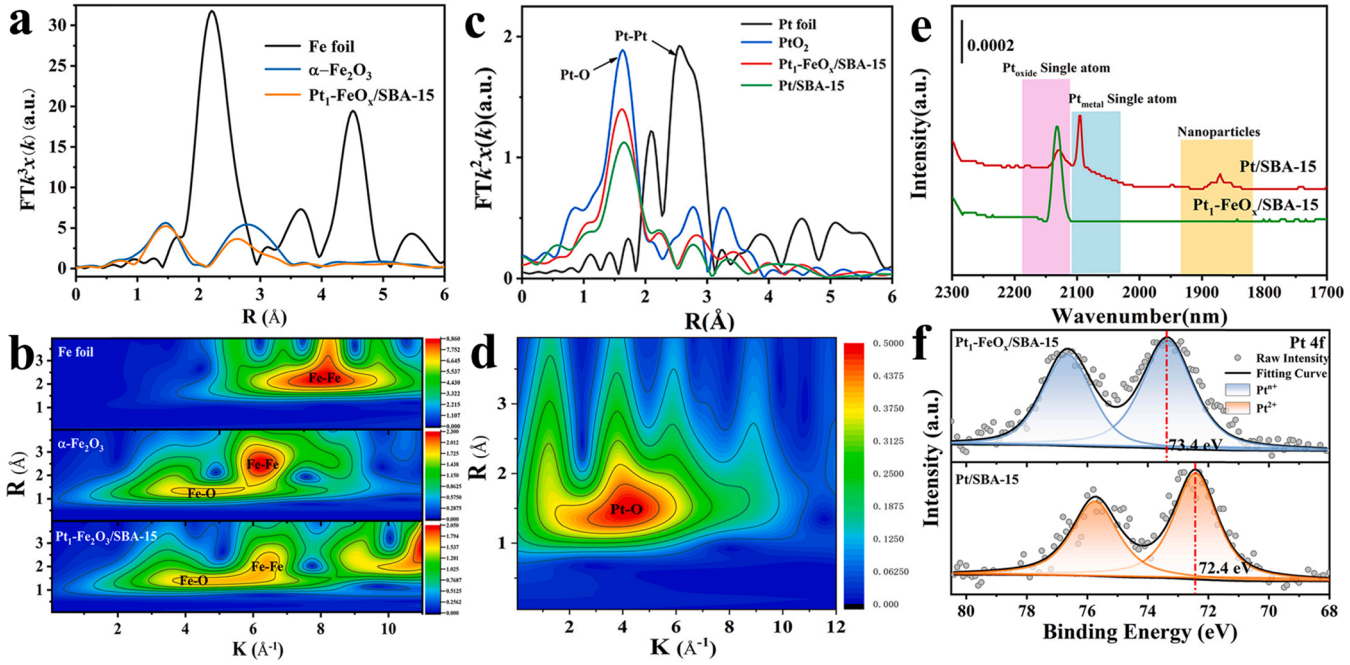

Fig. 3. Fe K edge (a) and Pt L_3 edge (c) EXAFS spectra in R space for samples. (b, d) Wavelet transform analysis of (b) Fe, α-Fe_2O_3, Pt_1/Fe_2O_3/SBA-15 and (d) Pt_1-FeO_x/SBA-15. (e) CO-DRIFT spectra for catalysts. (f) Pt 4f XPS of Pt_1-FeO_x/SBA-15 and Pt/SBA-15.

are bonded with oxygen, also as evidenced by the wavelet transforms of the Pt_1-FeO_x/SBA-15 (Fig. 3d). The EXAFS fitting results (Table S3) uncover that the CN of the single-Pt sites is approximately 5, indicating the FeO_x species strongly interact with the isolated Pt species [55]. The Pt-O path (R of 2.03 Å) and Pt-Pt path (R of 2.09 Å) are both observed in the Pt/SBA-15 with CN of 3.8 and 1.4, respectively, meaning that the Pt clusters were formed over catalyst [56], as proved by the HAADF-STEM images (Fig. 2c–f)).

The dispersion and coordination geometry of Pt in the catalyst were further performed by in-situ CO-DRIFTS (Fig. 3e). Pt_1-FeO_x/SBA-15 only exhibited a single strong peak at 2132 cm^{-1}, associated with the stretching vibrations of linearly bonded CO on single-atom Pt with the highly oxidized state [57]. However, Pt/SBA-15 arose two additional peaks at 2094 cm^{-1} and 1850 cm^{-1}, which was associated with the stretching vibrations of linearly bonded CO on Pt single-atoms in low-coordination mode, and the stretching vibrations of CO on Pt nanoparticles, respectively [58]. These results demonstrated that the FeO_x species noticeably improved the dispersion, and tailored the electronic configuration of platinum, which is agreement with TEM and EXAFS results.

XANES spectra (Fig. S8) showed that the white line intensities of Pt_1-FeO_x/SBA-15 and Pt/SBA-15 were both between the strengths of Pt and PtO_2, indicating that the Pt species were maintain the highly oxidized state. The chemical state of Pt species in Fe-containing and pristine SBA-15 were further investigated by XPS (Fig. 3f). Compared with Pt/SBA-15, the binding energy of Pt in Pt_1-FeO_x/SBA-15 shifted to a higher value with two bands at 73.4 eV and 72.4 eV, corresponding to the $4f_{7/2}$ of Pt^{n+} ($2.5 > n > 3.5$) and Pt^{2+}, respectively [3], indicating the strong interaction between Pt and FeO_x in Pt_1-FeO_x/SBA-15. The isolated Pt species with high surface positive charge may have a strong adsorption capacity toward C═O group, tending to improve the C═O bond selective hydrogenation in UAL [23,59].

In addition, the universality of this synthetic approach for other noble metal SACs was also probed. FeO_x/SBA-15 supported Pd, Rh, and Ir SACs could also be successfully obtained by hydrolysis of $Pd(acac)_2$, $Rh(acac)_3$, and $Ir(acac)_3$, respectively. These noble metals were well dispersed in an atomic level on the support, as clearly evidenced by HRTEM (Fig. S9), HAADF-STEM and CO-DRIFT (Fig. S10) [60,61], in which the large number of atomic dispersion of Pd, Rh, and Ir species (yellow circles) on FeO_x/SBA-15 was observed.

3.3. Catalytic performance in selective hydrogenation of UAL

The series of Pt-based catalysts were evaluated for the CAL (a typical substance of UAL) hydrogenation (Table 1). The $Pt(acac)_2$ precursor and FeO_x/SBA-15 support both proved to be catalytically inactive for hydrogenation of CAL. After the $Pt(acac)_2$ impregnated on support was hydrolyzed, Pt/SBA-15 had the poor selectivity (30.4 %) toward COL at 37 % CAL conversion under reaction conditions (room temperature, 9 h). Interestingly, Pt_1-FeO_x/SBA-15 exhibited a markedly high selectivity (95.2 %) toward COL at 100 % CAL conversion, indicating that the efficient removal of ligands in $Pt(acac)_2$ through hydrolysis led to the CAL hydrogenation activity over Pt species, and the combination of Pt and FeO_x on support contributed to the significantly high selectivity of COL. Compared with Pt/SBA-15, the introduced FeO_x nanoclusters could anchor Pt species and enabled them to dispersed at atomical-level, leading to a high catalytic activity that was often observed in the hydrogenation reaction over Pt SACs [22,62].

Among the reported Pt-base catalysts, the target product of COL in CAL hydrogenation tended to be further hydrogenated to hydrocinnamyl alcohol (HCOL) at a high CAL conversion [1,3]. Herein, the

Table 1
Catalytic performance in the CAL selective hydrogenation over various catalysts.

Catalysts[a]	Conv. (%)	Sele. (%)			TOF $_{(COL)}$ [b] (h^{-1})
		COL	HCAL	HCOL	
1 %Pt_1-FeO_x/SBA-15	100	95.2	1.7	3.1	128
1 %Pt/SBA-15	37.4	30.4	55.3	14.3	51
2 %Pt-FeO_x/SBA-15	100.0	89.6	3.8	2.6	124
3 %Pt-FeO_x/SBA-15	100.0	71.5	3.7	24.8	70
$Pt(acac)_2$	0	–	–	–	–
FeO_x/SBA-15	0	–	–	–	–

[a] Reaction conditions: 0.02 g catalyst; 25 mmol CAL; 3.0 MPa initial H_2 pressure; 5 mL i-PrOH; 600 rpm; 9 h and room temperature.

[b] $TOF_{(COL)}$ is denoted as the obtained amount of COL per molar amount of Pt converted per unit time at low conversion rate. (COL Pt^{-1} h^{-1})

high selectivity (95 %) of COL could be well maintained while the CAL was completely converted over Pt_1-FeO_x/SBA-15. Even the reaction time was further prolonged to 48 h after the total conversion of CAL (9 h), as shown in Fig. 4a, only slight drop was observed in the selectivity of COL (92.5 %), ranking it the best performed catalysts reported to date (Table S4). To rule out the possibility that the inhibition on deep hydrogenation was caused by the deactivation of catalysts, the further experiments were performed by adding the additional CAL to the above system (Fig. S11). The study found that CAL still reached 100 % conversion with the COL selectivity of 94 % after 10 h of reaction, certifying that the deactivation was not occurred in Pt_1-FeO_x/SBA-15 during the whole hydrogenation process. The reusability of the Pt_1-FeO_x/SBA-15 catalyst was assessed by performing the reactions over the used catalyst (Fig. S12). The minor drop in CAL conversion over subsequent reactions, may simply be attributed to a minor decrease in the amount of catalyst owing to the losses during the work-up and recycling process. It can be found that there is no distinct loss in selectivity towards COL after three cycles. To assess any Pt leached during the reaction, the post reaction solution was analyzed by ICP-AES, and the leach of Pt was not detected, confirming that the strong interaction between Pt and FeO_x. The highly dispersed Pt in Pt_1-FeO_x/SBA-15 after reaction was also evidenced by CO-DRIFT (Fig. S13), indicating that the Pt_1-FeO_x/SBA-15 catalyst was robust under the reaction conditions. To confirm the universality of chemoselectivity, the similar substances were also employed for test over Pt_1-FeO_x/SBA-15 (Fig. 4b). The catalytic results demonstrated that the target products of UOL exhibited extremely high selectivity (> 93 %) at a 100 % conversion of the tested substrates, and the high selectivity of UOL still maintained over the 48 h reaction time owing to the inhibition effects on deep hydrogenation. The conversion for various UAL over Pt_1-FeO_x/SBA-15 catalyst was related to their molecular structure, UAL with large R-substituent exhibited a relative low conversion because it is more difficult to approach the single-atom active sites.

To explore the synergism of Pt and FeO_x, in-situ DRIFT was performed using 3-methyl-2-butenal as probe molecules to investigate its adsorption state on the series of catalysts. The vibration in the spectrum of UAL showed two bands at 1681 cm^{-1} and 1666 cm^{-1}, which were ascribed to the vibrations of π-bonded (C═O) adsorption and η_1(C-O), respectively [63]. The bands at 1635/1616 cm^{-1} are assigned to the stretching vibrations C═C bond (Fig. 4c). It was found that the characteristic bands of probe molecule had slight changes after exposing on Pt/SBA-15 catalyst, however, the intensity of υ(C═O) over the FeO_x-based catalysts decreased with time on stream, the intensity of the C═O feature at 1681 cm^{-1} decreased more evidently over Pt_1-FeO_x/SBA-15. This result evidenced that the C═O group in the substrate preferred to linearly adsorb on single-atom Pt sites on Pt_1-FeO_x/SBA-15 through the π-bonded adsorption pattern (1681 cm^{-1}), and the C═O and C═C groups simultaneously adsorbed on the Pt sites in Pt/SBA-15 through the η_2 pattern [64]. Meanwhile the state of probe adsorbed on FeO_x/SBA-15 also revealed that the introduced FeO_x species preferentially adsorbed the C═O groups [65].

The adsorption of CAL and COL (target product) on Pt_1-FeO_x/SBA-15 were further investigate by density functional theory calculations (DFT), in which $Pt_1(OH)_2$ deposited on α-Fe_2O_3(001) surface was employed as the active sites by considering the spin-polarization effect (Fig. 5a). Differential charge density (Fig. 5b and Fig. S14) of catalyst indicated the charge of single-site Pt was depleted, and the abundant delocalized charges gathered along the Pt-O-Fe bond in Pt_1-FeO_x. Bader charge analysis revealed that the Pt atoms in the Pt_1-FeO_x system have 1.4 e^{-1} of electrons transferred to Fe along the Pt—O—Fe bond. Furthermore, considering the electrons transfer from Pt to Fe, the highly oxidized Pt species in a low spin state favor the adsorption of C═O groups. The C═O group in CAL molecule were adsorbed on Pt sites in a linear adsorption mode with adsorption energy (E_{ads}) of − 0.80 eV, and C═C group behaved in a horizontal adsorption mode with E_{ads} of − 0.68 eV (Fig. 5c and Fig. S15). The charge density difference of CAL adsorption on catalyst further confirmed the electron transfer of the C═O or the C═C group adsorbed on Pt sites (Fig. S16). Thus, the linearly adsorbed C═O groups in CAL molecule could be more favorable for hydrogenation on the Pt surface compared to C═C groups [66,67]. The adsorption state of the COL target molecular was also calculated on this model (Fig. 5d and Fig. S17), it was found that the -OH group in COL molecule had an E_{ads} of

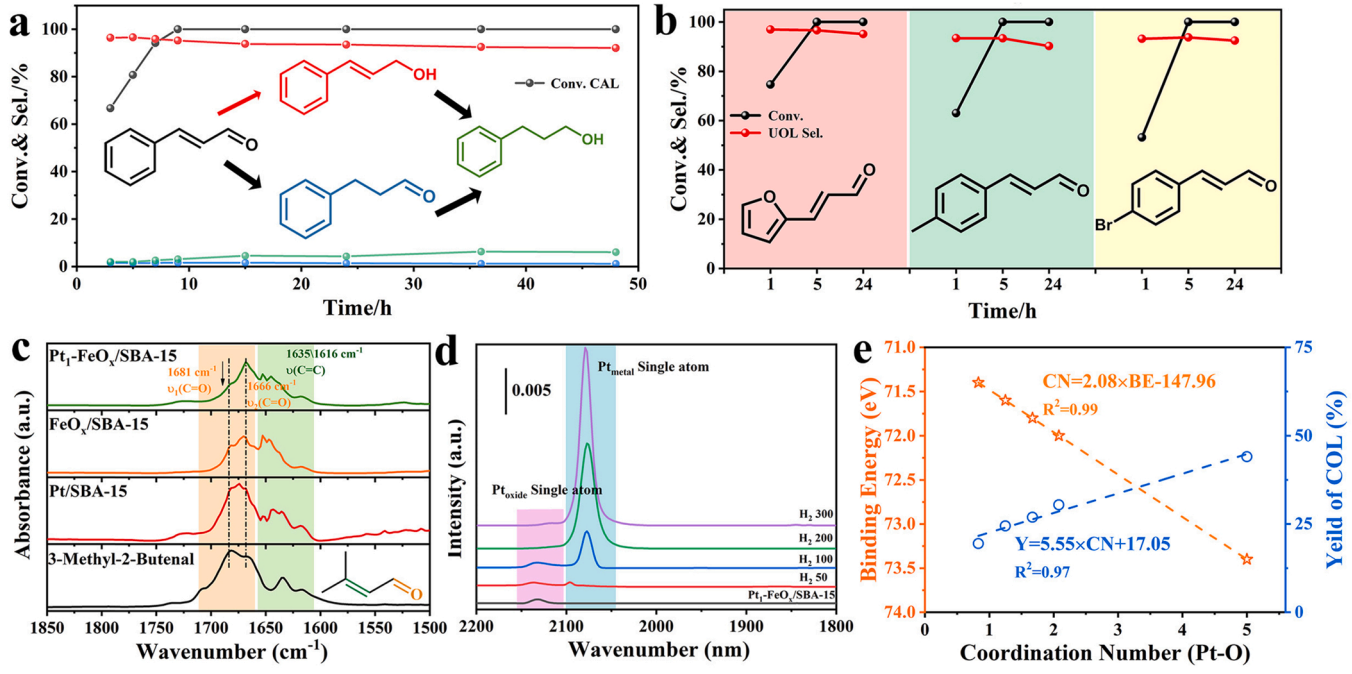

Fig. 4. (a) Catalytic results for CAL hydrogenation over 1 %Pt_1-FeO_x/SBA-15 at various reaction time. (Reaction conditions: 0.02 g catalyst; 25 mmol CAL; 3.0 MPa initial H_2 pressure; 5 mL i-PrOH; 600 rpm and RT) (b) Hydrogenation of different UAL by 1 %Pt_1-FeO_x/SBA-15. (The reaction conditions were identical to those in Fig. 4a.) (c) In-situ DRIFTS of 3-methyl-2-butenal absorbed on various catalysts. (d) CO-DRIFTS for 1 %Pt_1-FeO_x/SBA-15 catalysts after heat treatment at 10 vol% H_2/Ar. (e) The correlation between catalytic performance and coordination structure.

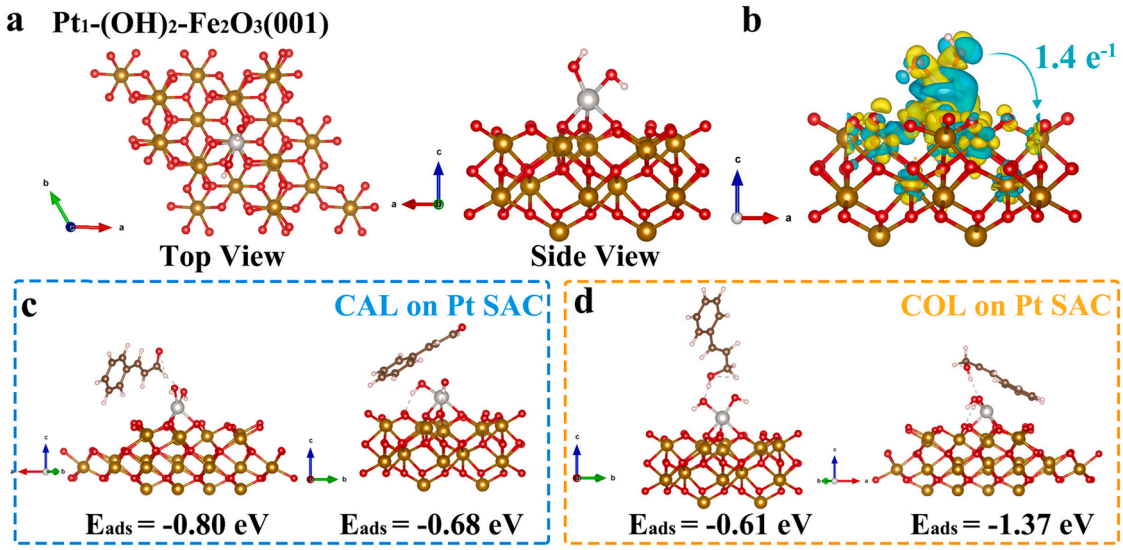

Fig. 5. (a) Optimized structures of Pt_1-$(OH)_2$-Fe_2O_3(001). White: H, brown: C, red: O, golden: Fe, silver: Pt. (b) Differential charge density of Pt_1-$(OH)_2$-Fe_2O_3(001), yellow represent electron accumulation and cyan represent electron depletion. (c) CAL adsorption on Pt_1-$(OH)_2$-Fe_2O_3(001) through C═O and C═C bond. (d) COL adsorption on Pt_1-$(OH)_2$-Fe_2O_3(001) through C—OH bond and Ph.

− 0.61 eV on Pt sites, and the aromatic group with an E_{ads} of − 1.37 eV. Owing to the large repulsion between the coordinated Pt species and the -OH group in the COL, the terminal -OH in the COL was away from the catalysts surface. In addition, the strong adsorption of aromatic group on Pt sites resulted in the difficulties for the C═C group to approach isolated Pt sites. Combing the experimental and calculated results, it was reasonable to believe that the C═O group preferential adsorption in CAL on Pt-FeO_x sites controlled the selectivity in the CAL hydrogenation, and the adverse adsorption model of the formed COL contributed to the markedly inhibition effect on the deep hydrogenation of COL.

Additionally, the Pt-FeO_x/SBA-15 with high Pt loading (2 and 3 wt %) still maintained the atomic-level dispersion, but some electron-rich single-atom $Pt^{\delta+}$ species were formed on them especially for 3 %Pt-FeO_x/SBA-15, as evidenced by CO-DRIFTS (Fig. S18) [58]. The catalytic results (Table 1) showed that the selectivity of COL was 90 % for 2 % Pt-FeO_x/SBA-15, and 72 % for 3 %Pt-FeO_x/SBA-15, revealing that the catalytic performance is closely related to the surface charge density of Pt single-atom [68,69]. To further verify the relationship between the Pt single-atom electronic configuration and selectivity, the typical 1 % Pt_1-FeO_x/SBA-15 catalyst was reduced to adjust the electronic structure of Pt under H_2 atmosphere with various temperatures, the platinum chemical state was examined by XPS (Fig. S19). With the enhancement of reduction temperature from 50 to 300 °C, the binding energy of Pt $4f_{7/2}$ was gradually decreased from 73.4 eV to 71.4 eV, reflecting that the surface of Pt species possessed more high electronic density. The chemical state of FeO_x species was not changed by such treatment (Fig. S20). Interestingly, CO-DRIFT spectra (Fig. 4d) collected on those catalysts evidenced that the Pt species could still maintain the single-atomic state after reduction, but the surface of Pt species became electric-rich. This series of catalysts were tested for the CAL hydrogenation, the catalytic results were listed in Table S5. Fig. 4e exhibits the relationship between the electronic configuration of Pt and the productivity of COL, where the orange line displayed the relationship between the CN and average valence state of Pt species (CN calculated by EXAFS and XPS) [70], and the blue line represented the relationship between the CN of Pt-O and the yield of COL under the low conversion of CAL. It was found that the CN of Pt-O displayed a well linear relationship with the yield of COL, and the high CN and oxidation state of Pt tended to an excellent productivity toward COL. Pt_1-FeO_x/SBA-15 after reduction at 300 °C had obvious drops in catalytic activity and initial selectivity for COL (Fig. S21), meanwhile, the selectivity of COL also decreased distinctly upon extending the reaction after the complete consumption of CAL. This result revealed that the highly oxidized Pt single-atoms was beneficial to the C═O group selective hydrogenation in CAL, and noticeably suppressed the further hydrogenation of the COL target molecular. Our finding clearly demonstrated the electronic configuration of Pt single-atom had an important role in the selectivity control for such complicated hydrogenation reactions.

4. Conclusions

In conclusion, we developed a facile strategy to fabricate the highly oxidized Pt SACs by pre-constructing highly dispersed FeO_x nanoclusters on SBA-15 material, and applying $Pt(acac)_2$ as a precursor. The organic ligands in $Pt(acac)_2$ averted the aggregation of Pt cations during the step of impregnation, and the gentle hydrolysis approach could efficiently remove the ligand and enable the platinum to atomically disperse on support, which is also applicable to fabrication of other noble metal SACs (i.e., Pd, Ir, and Rh). Significantly, Pt_1/Fe_2O_3/SBA-15 exhibited a remarkably high selectivity to COL (> 95 %) under the complete conversion of CAL, and further hydrogenation of the formed COL was obviously inhibited. The excellent catalytic performance for such reactions was ascribed to the combined effect between the isolated Pt atom with much surface positive charges and the FeO_x nanoclusters on SBA-15. This work clearly demonstrated that the single atom coupled with functional metal oxides nanoclusters is an applicable technique for catalyzing those complicated hydrogenation reactions, and our synthetic strategy also offered an optional approach for the rational design of SACs.

CRediT authorship contribution statement

Yu Liang: Experimental, Characterization, Writing – original draft. **Qiong Tang:** Investigation, Characterization. **Lei Liu:** Supervision, Methodology, Funding acquisition, Writing – review & editing. **Dingsheng Wang:** Formal analysis, Methodology. **Jinxiang Dong:** Supervision, Conceptualization.

Declaration of Competing Interest

The authors declare that they have no known competing financial interests or personal relationships that could have appeared to influence

the work reported in this paper.

Data Availability

Data will be made available on request.

Acknowledgments

This work was supported by the National Natural Science Foundation of China (U1910202 and 21978194), the Key Research and Development Program of Shanxi Province (202102090301005), and the Fund for Shanxi "1331 Project".

Author Contributions

The manuscript was written through contributions of all authors. All authors have given approval to the final version of the manuscript.

Supporting Information

Details of the experimental, characterization data (XRD, BET, TG-MS, UV-Vis, HPLC, XANES, TEM, and CO-DRIFT), catalytic performance results, and DFT calculations.

Appendix A. Supporting information

Supplementary data associated with this article can be found in the online version at doi:10.1016/j.apcatb.2023.122783.

References

[1] X. Lan, T. Wang, Highly selective catalysts for the hydrogenation of unsaturated aldehydes: a review, ACS Catal. 10 (2020) 2764–2790.
[2] P. Gallezot, D. Richard, Selective hydrogenation of α, β-unsaturated aldehydes, Catal. Rev. 40 (1998) 81–126.
[3] X. Wang, X. Liang, P. Geng, Q. Li, Recent advances in selective hydrogenation of cinnamaldehyde over supported metal-based catalysts, ACS Catal. 10 (2020) 2395–2412.
[4] Y. Wang, X. Rong, T. Wang, S. Wu, Z. Rong, Y. Wang, J. Qu, Influence of graphene surface chemistry on Ir-catalyzed hydrogenation of p-chloronitrobenzene and cinnamaldehyde: weak molecule-support interactions, J. Catal. 377 (2019) 524–533.
[5] J. Shi, R. Nie, P. Chen, Z. Hou, Selective hydrogenation of cinnamaldehyde over reduced graphene oxide supported Pt catalyst, Catal. Commun. 41 (2013) 101–105.
[6] Y. Tang, H. Li, K. Cui, Y. Xia, G. Yuan, J. Feng, W. Xiong, Chemoselective hydrogenation of cinnamaldehyde over amorphous coordination polymer supported Pt-Co bimetallic nanocatalyst, Chem. Phys. Lett. 801 (2022), 139683.
[7] P. Liu, Y.-L. Zhu, L. Zhou, W.-H. Zhang, Y.-X. Li, Amorphous nickel phosphide nanoparticles for selective hydrogenation of cinnamaldehyde, Catal. Lett. 150 (2020) 2695–2702.
[8] W. Zhang, H. Xin, Y. Zhang, X. Jin, P. Wu, W. Xie, X. Li, Bimetallic Pt-Fe catalysts supported on mesoporous TS-1 microspheres for the liquid-phase selective hydrogenation of cinnamaldehyde, J. Catal. 395 (2021) 375–386.
[9] I. Ro, I.B. Aragao, Z.J. Brentzel, Y. Liu, K.R. Rivera-Dones, M.R. Ball, D. Zanchet, G. W. Huber, J.A. Dumesic, Intrinsic activity of interfacial sites for Pt-Fe and Pt-Mo catalysts in the hydrogenation of carbonyl groups, Appl. Catal. B 231 (2018) 182–190.
[10] N.M. Bertero, A.F. Trasarti, B. Moraweck, A. Borgna, A.J. Marchi, Selective liquid-phase hydrogenation of citral over supported bimetallic Pt–Co catalysts, Appl. Catal. A 358 (2009) 32–41.
[11] K. Wang, X. He, J.-C. Wang, X. Liang, Highly stable Pt–Co bimetallic catalysts prepared by atomic layer deposition for selective hydrogenation of cinnamaldehyde, Nanotechnology 33 (2022), 215602.
[12] X. Wang, Y. He, Y. Liu, J. Park, X. Liang, Atomic layer deposited Pt-Co bimetallic catalysts for selective hydrogenation of α, β-unsaturated aldehydes to unsaturated alcohols, J. Catal. 366 (2018) 61–69.
[13] Z. Gao, L. Cai, C. Miao, T. Hui, Q. Wang, D. Li, J. Feng, Electronic metal-support interaction strengthened Pt/CoAl-LDHs catalyst for selective cinnamaldehyde hydrogenation, ChemCatChem 14 (2022), e202200634.
[14] Z. Wei, X. Zhu, X. Liu, H. Xu, X. Li, Y. Hou, Y. Liu, Pt-Re/rGO bimetallic catalyst for highly selective hydrogenation of cinnamaldehyde to cinnamylalcohol, Chin. J. Chem. Eng. 27 (2019) 369–378.
[15] H. Rong, Z. Niu, Y. Zhao, H. Cheng, Z. Li, L. Ma, J. Li, S. Wei, Y. Li, Structure evolution and associated catalytic properties of Pt Sn bimetallic nanoparticles, Chem. - Eur. J. 21 (2015) 12034–12041.
[16] L.-X. Dai, W. Zhu, M. Lin, Z.-P. Zhang, J. Gu, Y.-H. Wang, Y.-W. Zhang, Self-supported composites of thin Pt–Sn crosslinked nanowires for the highly chemoselective hydrogenation of cinnamaldehyde under ambient conditions, Inorg. Chem. Front. 2 (2015) 949–956.
[17] C. Dietrich, D. Schild, W. Wang, C. Kübel, S. Behrens, Bimetallic Pt/Sn-based nanoparticles in ionic liquids as nanocatalysts for the selective hydrogenation of cinnamaldehyde, Z. Anorg. Allg. Chem. 643 (2017) 120–129.
[18] X.-F. Yang, A. Wang, B. Qiao, J. Li, J. Liu, T. Zhang, Single-atom catalysts: a new frontier in heterogeneous catalysis, Acc. Chem. Res. 46 (2013) 1740–1748.
[19] T.-N. Ye, Z. Xiao, J. Li, Y. Gong, H. Abe, Y. Niwa, M. Sasase, M. Kitano, H. Hosono, Stable single platinum atoms trapped in sub-nanometer cavities in $12CaO{\cdot}7Al_2O_3$ for chemoselective hydrogenation of nitroarenes, Nat. Commun. 11 (2020) 1–10.
[20] X. He, Q. He, Y. Deng, M. Peng, H. Chen, Y. Zhang, S. Yao, M. Zhang, D. Xiao, D. Ma, A versatile route to fabricate single atom catalysts with high chemoselectivity and regioselectivity in hydrogenation, Nat. Commun. 10 (2019) 1–9.
[21] H. Wei, X. Liu, A. Wang, L. Zhang, B. Qiao, X. Yang, Y. Huang, S. Miao, J. Liu, T. Zhang, FeO_x-supported platinum single-atom and pseudo-single-atom catalysts for chemoselective hydrogenation of functionalized nitroarenes, Nat. Commun. 5 (2014) 1–8.
[22] Z. Sun, S. Wang, W. Chen, Metal single-atom catalysts for selective hydrogenation of unsaturated bonds, J. Mater. Chem. A 9 (2021) 5296–5319.
[23] B. Zhang, H. Asakura, J. Zhang, J. Zhang, S. De, N. Yan, Stabilizing a $platinum_1$ single-atom catalyst on supported phosphomolybdic acid without compromising hydrogenation activity, Angew. Chem. 128 (2016) 8459–8463.
[24] K. Qi, M. Chhowalla, D. Voiry, Single atom is not alone: metal–support interactions in single-atom catalysis, Mater. Today 40 (2020) 173–192.
[25] C. Rivera-Cárcamo, C. Scarfiello, A.B. García, Y. Tison, H. Martinez, W. Baaziz, O. Ersen, C. Le Berre, P. Serp, Stabilization of metal single atoms on carbon and TiO_2 supports for CO_2 hydrogenation: the importance of regulating charge transfer, Adv. Mater. Interfaces 8 (2021), 2001777.
[26] R. Lang, X. Du, Y. Huang, X. Jiang, Q. Zhang, Y. Guo, K. Liu, B. Qiao, A. Wang, T. Zhang, Single-atom catalysts based on the metal–oxide interaction, Chem. Rev. 120 (2020) 11986–12043.
[27] D. Liu, Q. He, S. Ding, L. Song, Structural regulation and support coupling effect of single-atom catalysts for heterogeneous catalysis, Adv. Energy Mater. 10 (2020), 2001482.
[28] J. Shan, C. Ye, Y. Jiang, M. Jaronice, Y. Zheng, S.Z. Qiao, Metal-metal interactions in correlated single-atom catalysts, Sci. Adv. 8 (2022) eabo0762.
[29] Y. Ying, X. Luo, J. Qiao, H. Huang, "More is different:" synergistic effect and structural engineering in double-atom catalysts, Adv. Funct. Mater. 31 (2021), 2007423.
[30] L. Liu, A.Corma Metal, catalysts for heterogeneous catalysis: from single atoms to nanoclusters and nanoparticles, Chem. Rev. 118 (2018) 4981–5079.
[31] B. Qiao, A. Wang, X. Yang, L.F. Allard, Z. Jiang, Y. Cui, J. Liu, J. Li, T. Zhang, Single-atom catalysis of CO oxidation using Pt_1/FeO_x, Nat. Chem. 3 (2011) 634–641.
[32] P. Du, R. Qi, Y. Zhang, Q. Gu, X. Xu, Y. Tan, X. Liu, A. Wang, B. Zhu, B. Yang, Single-atom-driven dynamic carburization over Pd_1–FeO_x catalyst boosting CO_2 conversion, Chem 8 (2022) 3252–3262.
[33] Y. Xin, N. Zhang, Y. Lv, J. Wang, Q. Li, Z. Zhang, From nanoparticles to single atoms for Pt/CeO_2: synthetic strategies, characterizations and applications, J. Rare Earths 38 (2020) 850–862.
[34] Y. Lu, S. Zhou, C.-T. Kuo, D. Kunwar, C. Thompson, A.S. Hoffman, A. Boubnov, S. Lin, A.K. Datye, H. Guo, Unraveling the intermediate reaction complexes and critical role of support-derived oxygen atoms in CO oxidation on single-atom Pt/CeO_2, ACS Catal. 11 (2021) 8701–8715.
[35] J. Park, S. Lee, H.E. Kim, A. Cho, S. Kim, Y. Ye, J.W. Han, H. Lee, J.H. Jang, J. Lee, Investigation of the support effect in atomically dispersed Pt on WO_{3-x} for utilization of Pt in the hydrogen evolution reaction, Angew. Chem. Int. Ed. 58 (2019) 16038–16042.
[36] T. Chu, C. Rong, L. Zhou, X. Mao, B. Zhang, F. Xuan, Progress and perspectives of single-atom catalysts for gas sensing, Adv. Mater. 35 (2022), 2206783.
[37] B. Han, Y. Guo, Y. Huang, W. Xi, J. Xu, J. Luo, H. Qi, Y. Ren, X. Liu, B. Qiao, Strong metal–support interactions between Pt single atoms and TiO_2, Angew. Chem. Int. Ed. 59 (2020) 11824–11829.
[38] S. Hoang, Y. Guo, A.J. Binder, W. Tang, S. Wang, J.J. Liu, H. Tran, X. Lu, Y. Wang, Y. Ding, Activating low-temperature diesel oxidation by single-atom Pt on TiO_2 nanowire array, Nat. Commun. 11 (2020) 1–10.
[39] W.H. Li, J. Yang, D. Wang, Long-range interactions in diatomic catalysts boosting electrocatalysis, Angew. Chem. Int. Ed. (2022), e202213318.
[40] X. Zheng, B. Li, Q. Wang, D. Wang, Y. Li, Emerging low-nuclearity supported metal catalysts with atomic level precision for efficient heterogeneous catalysis, Nano Res. 15 (2022) 7806–7839.
[41] D. Ma, Z. Zeng, L. Liu, X. Huang, Y. Jia, Computational evaluation of electrocatalytic nitrogen reduction on TM single-, double-, and triple-atom catalysts (TM = Mn, Fe, Co, Ni) based on graphdiyne monolayers, J. Phys. Chem. C 123 (2019) 19066–19076.
[42] P. Zhu, X. Xiong, D. Wang, Regulations of active moiety in single atom catalysts for electrochemical hydrogen evolution reaction, Nano Res. 15 (2022) 1–24.
[43] X. Li, X.I. Pereira-Hernández, Y. Chen, J. Xu, J. Zhao, C.-W. Pao, C.-Y. Fang, J. Zeng, Y. Wang, B.C. Gates, Functional CeOx nanoglues for robust atomically dispersed catalysts, Nature 611 (2022) 284–288.
[44] T. Cui, Y.P. Wang, T. Ye, J. Wu, Z. Chen, J. Li, Y. Lei, D. Wang, Y. Li, Engineering dual single-atom sites on 2D ultrathin N-doped carbon nanosheets attaining ultra-low-temperature zinc-air battery, Angew. Chem. Int. Ed. 61 (2022), e202115219.

[45] X. He, Y. Deng, Y. Zhang, Q. He, D. Xiao, M. Peng, Y. Zhao, H. Zhang, R. Luo, T. Gan, Mechanochemical kilogram-scale synthesis of noble metal single-atom catalysts, Cell Rep. Phys. Sci. 1 (2020), 100004.
[46] Y. Liu, X. Wu, Z. Li, J. Zhang, S.-X. Liu, S. Liu, L. Gu, L.R. Zheng, J. Li, D. Wang, Fabricating polyoxometalates-stabilized single-atom site catalysts in confined space with enhanced activity for alkynes diboration, Nat. Commun. 12 (2021) 1–9.
[47] S.B. Hong, E. Mielczarski, M.E. Davis, Aromatization of n-hexane by platinum-containing molecular sieves I. Catalyst preparation by the vapor phase impregnation method, J. Catal. 134 (1992) 349–358.
[48] J. Jones, H. Xiong, A.T. DeLaRiva, E.J. Peterson, H. Pham, S.R. Challa, G. Qi, S. Oh, M.H. Wiebenga, X.I. Pereira Hernández, Thermally stable single-atom platinum-on-ceria catalysts via atom trapping, Science 353 (2016) 150–154.
[49] M. Kruk, M. Jaroniec, C.H. Ko, R. Ryoo, Characterization of the porous structure of SBA-15, Chem. Mater. 12 (2000) 1961–1968.
[50] S. Musić, A. Šarić, Formation of hollow ZnO particles by simple hydrolysis of zinc acetylacetonate, Ceram. Int. 38 (2012) 6047–6052.
[51] H. Uchiyama, K. Takagi, H. Kozuka, Solvothermal synthesis of size-controlled ZrO_2 microspheres via hydrolysis of alkoxides modified with acetylacetone, Colloids Surf. A 403 (2012) 121–128.
[52] X. Zhang, X. Han, Z. Jiang, J. Xu, L. Chen, Y. Xue, A. Nie, Z. Xie, Q. Kuang, L. Zheng, Atomically dispersed hierarchically ordered porous Fe–N–C electrocatalyst for high performance electrocatalytic oxygen reduction in Zn-Air battery, Nano Energy 71 (2020), 104547.
[53] M. Chen, H. Yin, X. Li, Y. Qiu, G. Cao, J. Wang, X. Yang, P. Wang, Facet-and defect-engineered Pt/Fe_2O_3 nanocomposite catalyst for catalytic oxidation of airborne formaldehyde under ambient conditions, J. Hazard. Mater. 395 (2020), 122628.
[54] A. Siani, O.S. Alexeev, G. Lafaye, M.D. Amiridis, The effect of Fe on SiO_2-supported Pt catalysts: structure, chemisorptive, and catalytic properties, J. Catal. 266 (2009) 26–38.
[55] R. Gao, J. Wang, Z.-F. Huang, R. Zhang, W. Wang, L. Pan, J. Zhang, W. Zhu, X. Zhang, C. Shi, Pt/Fe_2O_3 with Pt–Fe pair sites as a catalyst for oxygen reduction with ultralow Pt loading, Nat. Energy 6 (2021) 614–623.
[56] M.A. Gawish, Q. Drmosh, S.A. Onaizi, Single atom catalysts: an overview of the coordination and interactions with metallic supports, Chem. Rec. 22 (2022), e202100328.
[57] L. DeRita, S. Dai, K. Lopez-Zepeda, N. Pham, G.W. Graham, X. Pan, P. Christopher, Catalyst architecture for stable single atom dispersion enables site-specific spectroscopic and reactivity measurements of CO adsorbed to Pt atoms, oxidized Pt clusters, and metallic Pt clusters on TiO_2, J. Am. Chem. Soc. 139 (2017) 14150–14165.
[58] L. Zhang, K. Doyle-Davis, X. Sun, Characterization of supported metal single-atom catalysts, Support. Met. Single At. Catal. (2022) 169–198.
[59] Z. Zhang, Y. Zhu, H. Asakura, B. Zhang, J. Zhang, M. Zhou, Y. Han, T. Tanaka, A. Wang, T. Zhang, Thermally stable single atom $Pt/m\text{-}Al_2O_3$ for selective hydrogenation and CO oxidation, Nat. Commun. 8 (2017) 1–10.
[60] H. Jeong, G. Lee, B.-S. Kim, J. Bae, J.W. Han, H. Lee, Fully dispersed Rh ensemble catalyst to enhance low-temperature activity, J. Am. Chem. Soc. 140 (2018) 9558–9565.
[61] J. Fu, J. Dong, R. Si, K. Sun, J. Zhang, M. Li, N. Yu, B. Zhang, M.G. Humphrey, Q. Fu, Synergistic effects for enhanced catalysis in a dual single-atom catalyst, ACS Catal. 11 (2021) 1952–1961.
[62] J. Zhang, H. Zhang, Y. Wu, C. Liu, Y. Huang, W. Zhou, B. Zhang, Single-atom catalysts for thermal-and electro-catalytic hydrogenation reactions, J. Mater. Chem. A 10 (2022) 5743–5757.
[63] Y. Bonita, V. Jain, F. Geng, T.P. O'Connell, N.X. Ramos, N. Rai, J.C. Hicks, Hydrogenation of cinnamaldehyde to cinnamyl alcohol with metal phosphides: catalytic consequences of product and pyridine doping, Appl. Catal. B 277 (2020), 119272.
[64] B. Bachiller-Baeza, I. Rodrıguez-Ramos, A. Guerrero-Ruiz, Influence of Mg and Ce addition to ruthenium based catalysts used in the selective hydrogenation of α, β-unsaturated aldehydes, Appl. Catal. A 205 (2001) 227–237.
[65] L. Kuai, Z. Chen, S. Liu, E. Kan, N. Yu, Y. Ren, C. Fang, X. Li, Y. Li, B. Geng, Titania supported synergistic palladium single atoms and nanoparticles for room temperature ketone and aldehydes hydrogenation, Nat. Commun. 11 (2020) 1–9.
[66] Y. Liang, M. Douthwaite, X. Huang, B. Zhao, Q. Tang, L. Liu, J. Dong, Zero-oxidation state precursor assisted fabrication of highly dispersed and stable Pt catalyst for chemoselective hydrogenation of α, β-unsaturated aldehydes, Nano Res. (2022).
[67] W.O. Oduro, N. Cailuo, K.M.K. Yu, H. Yang, S.C. Tsang, Geometric and electronic effects on hydrogenation of cinnamaldehyde over unsupported Pt-based nanocrystals, Phys. Chem. Chem. Phys. 13 (2011) 2590–2602.
[68] Y. Pan, Y. Qian, X. Zheng, S.-Q. Chu, Y. Yang, C. Ding, X. Wang, S.-H. Yu, H.-L. Jiang, Precise fabrication of single-atom alloy co-catalyst with optimal charge state for enhanced photocatalysis, Natl. Sci. Rev. 8 (2021) nwaa224.
[69] J. Fan, Y. Zhao, H. Du, L. Zheng, M. Gao, D. Li, J. Feng, Light-Induced structural dynamic evolution of Pt single atoms for highly efficient photocatalytic CO_2 reduction, ACS Appl. Mater. Interfaces 14 (2022) 26752–26765.
[70] L. Wang, C. Zhu, M. Xu, C. Zhao, J. Gu, L. Cao, X. Zhang, Z. Sun, S. Wei, W. Zhou, Boosting activity and stability of metal single-atom catalysts via regulation of coordination number and local composition, J. Am. Chem. Soc. 143 (2021) 18854–18858.